AFM tip-based nanomachining with increased cutting speed at the tool-workpiece interface

Yanquan Geng[1,2], Emmanuel B. Brousseau[1,*], Xuesen Zhao[1,2], M. Gensheimer[1], C.R. Bowen[3]

[1] *Cardiff School of Engineering, Cardiff University, Cardiff, United Kingdom*

[2] *Center for Precision Engineering, Harbin Institute of Technology, Harbin, China*

[3] *Department of Mechanical Engineering, University of Bath, Bath, United Kingdom*

Abstract

This paper reports a study towards enhancing the throughput of the Atomic Force Microscopy (AFM) tip-based nanomachining process by increasing the cutting speed at the interface between the tool and the workpiece. A modified AFM set-up was implemented, which combined the fast reciprocating motions of a piezoelectric actuator, on which the workpiece was mounted, and the linear displacement of the AFM stage, which defined the length of produced grooves. The influence of the feed, the feed direction and the cutting speed on the machined depth and on the chip formation was studied in detail when machining poly(methyl methacrylate). A theoretical cutting speed over 5 m/min could be achieved with this set-up when the frequency of the piezoelectric actuator reciprocating motions was 40 kHz. This is significantly better than the state of the art for AFM-based nanomachining, which is currently less than 1 m/min.

Keywords: Atomic force microscopy, Tip-based nanomachining, Piezoelectric actuation.

1. Introduction

Machining nano-scale features with the tip of an Atomic Force Microscope (AFM) probe has been extensively studied in the past two decades and has been reported in recent reviews on nanofabrication techniques enabled by AFM instrumentation [1-3]. From a manufacturing perspective, the AFM tip-based nanomachining process exhibits a number of attractive advantages, which can be summarised as follows. Firstly, the approach does not rely on capital-intensive equipment. Secondly, it can be applied on a wide range of workpiece materials. Finally, it is relatively straight-forward to implement since successive exposure and etching steps can be avoided, which are otherwise needed with photolithography-based approaches. Thus, it could be argued that AFM tip-based nanomachining represents a potential alternative to current vacuum and mask-based fabrication techniques, which are the *de facto* standard when producing nano-electro-mechanical systems components and related semi-conductor devices.

Despite these advantages, this mechanical machining approach is not yet considered as a serious competitor for nano-scale manufacturing. This is partly due to its relatively low processing speed [4]. Indeed, the vast majority of AFM tip-based nanomachining investigations are reported to operate at cutting speeds below 1

mm/min [5-7]. In an effort to overcome this limitation, researchers from the micro- and nano-manufacturing community have recently attempted to increase the speed of this particular process. As will be described below, these advances essentially rely on the development of specific solutions for the generation of the relative motion between the AFM tip and the workpiece. In spite of these recent developments, to the best knowledge of the authors, the highest cutting speed achieved at the tip-workpiece interface to date is still less than 1 m/min. This is in contrast to values routinely reached with single point diamond turning (SPDT), where cutting speeds of 10-100 m/min [8, 9] and even over 500 m/min [10] are reported. Despite the differences in the type of structures produced by AFM tip-based nanomachining and SPDT as mentioned in [11], it is of interest to compare these two processes as they share similarities in terms of the mechanics of the cutting process at the tool-workpiece interface. While AFM nanomachining is currently limited to less than 1 m/min, it should be noted that the state-of-the-art in AFM imaging has demonstrated tip scanning speed values over 10 m/min. Indeed, the pioneering work of Humphris *et al* (2005) [12] and Picco *et al* (2007) [13] has enabled the development of the so-called "high-speed atomic force microscopy" technique for recording AFM images with high acquisition rates.

Thus, it is argued that there remains scope to further accelerate the AFM tip-based nanomachining process. An early effort in this direction was presented by Yan and co-workers [14] who achieved a machining speed of 6 mm/min by retrofitting an ultra-precision stage in a commercial AFM instrument. A few years later, Bourne *et al*

developed a custom AFM head assembly, which could be set-up on a five-axis microscale machine tool platform in place of the spindle assembly [5]. Using this platform, a cutting speed of 25 mm/min was reported. Recently, Brousseau *et al* achieved a cutting speed of 32 mm/min by implementing a hybrid process that combined roll-to-roll and AFM technologies [15]. Despite the potential of this particular solution to reach higher cutting speeds, its limitation is that it is only able to machine polymer sheets a few tens of micrometres thick and to cut long grooves, rather than produce discrete features.

Based only on the dimensions of produced grooves, the highest cutting speed achieved at the tip-workpiece interface to date is estimated to be 301 mm/min. This was realised in the study from Gozen and Ozdoganlar [16]. It should be noted that, as with Bourne *et al*, this work was not implemented on a standard AFM instrument. In this case, a customised system was developed where the AFM probe was used as a rigid cutting tool and where piezoelectric actuators enabled the generation of rotational motions, either in-plane or out-of-plane, between the tip and the workpiece. The implementation of in-plane rotational displacements of the workpiece based on piezoelectric actuation has also recently been investigated by other researchers [17, 18]. In this way, Zhang and Dong achieved a cutting speed of 254 mm/min [17] while Park and co-workers reported experimental trials, which reached values of approximately 50 mm/min [18]. Interestingly, both of these studies demonstrated the possibility to integrate a customised stage based on piezoelectric actuation onto a commercial AFM instrument. The advantage of such an approach is that it can be

transferred relatively easily to standard AFM equipment.

In this context, the motivation behind the research reported in this paper is to attain cutting speed values at the tip-workpiece interface in excess of 1 m/min, i.e. about one order of magnitude higher than the state-of-the-art. In a similar way to a number of previous studies, it is proposed to exploit piezoelectric actuation to generate rapid and high frequency motion of the workpiece. It is also proposed to implement this approach on a commercial AFM instrument, such that the solution may be realised relatively easily by a large number of AFM practitioners.

The paper is organised as follows. The next section describes the experimental set-up employed in this study to perform the AFM tip-based nanomachining experiments and also to conduct the dynamic characterisation of the piezoelectric actuator utilised. Then, nanomachining outcomes observed when processing a poly(methyl methacrylate) (PMMA) substrate are reported and discussed in light of the different parameters used. In particular, the influence of the feed, the feed direction and the cutting speed on the machined depth and on the chip formation is examined in detail. Finally, conclusions and outlook for future work are presented in the last section.

2. Experimental methodology

2.1. Nanomachining set-up and procedure

Figure 1 (a) shows a schematic view of the modified AFM set-up which was

implemented in this work to realise tip-based nanomachining operations with increased cutting speed. The developed set-up relied on a commercial AFM (XE-100, Park Systems, Korea) and on a unidirectional shear-type piezoelectric actuator (NAC2402-H2.3, Noliac, Denmark). This actuator was placed on the original stage of the AFM system, which had a maximum displacement range of 45 μm by 45 μm. The purpose of the shear-type actuator was to generate linear reciprocal displacements of the workpiece at high frequency (i.e. until 40 kHz). This defined the scratching direction and the amplitude of this reciprocating motion defined the groove width. At the same time, the tip followed a predefined linear trajectory along the length of a groove to be machined. This trajectory was controlled via the motion of the AFM stage and established the feed direction.

A diamond three-sided pyramidal AFM tip (DNISP, Bruker, Germany) was used for all nanomachining operations in this work. The normal spring constant of the cantilever, on which the tip is mounted, was specified to be 221 N/m by the manufacturer. Due to the non-axisymmetric geometry of the tip, different feed and/or scratching directions can lead to various machining outcomes. The typical relative directions of the tip motion found in conventional AFM tip-based nanomachining are shown in Figures 1 (b)-(d). When considering the addition of reciprocating motions as implemented in this study, three typical combinations of feed and scratch directions can be studied:

(i) The linear movement of the AFM stage is parallel and towards the cantilever of the

probe. The relative motion of the tip related to the sample is denoted as V_{tip} and is shown in Figure 1 (b). In this study, such a configuration is defined as the 'edge-forward' feed direction.

(ii) The linear movement of the AFM stage is parallel and away from the probe. In this case, the relative motion of the tip related to the sample, i.e. V_{tip}, is as shown in Figure 1 (c). This configuration is denoted as the 'face-forward' feed direction. In cases (i) and (ii), the reciprocating motion of sample generated by the piezoelectric actuator is conducted in a direction that is perpendicular to the long axis of the cantilever, which is denoted as V_{sample} as shown in Figures 1 (b) and (c).

(iii) The movement of the AFM stage is perpendicular to the cantilever. This means that the relative motion of the tip to the sample can be described by V_{tip} as illustrated in Figure 1 (d). This case is defined as the 'side-forward' feed direction. In this configuration, the reciprocating motion of the sample, V_{sample}, is carried out along the long axis of the cantilever.

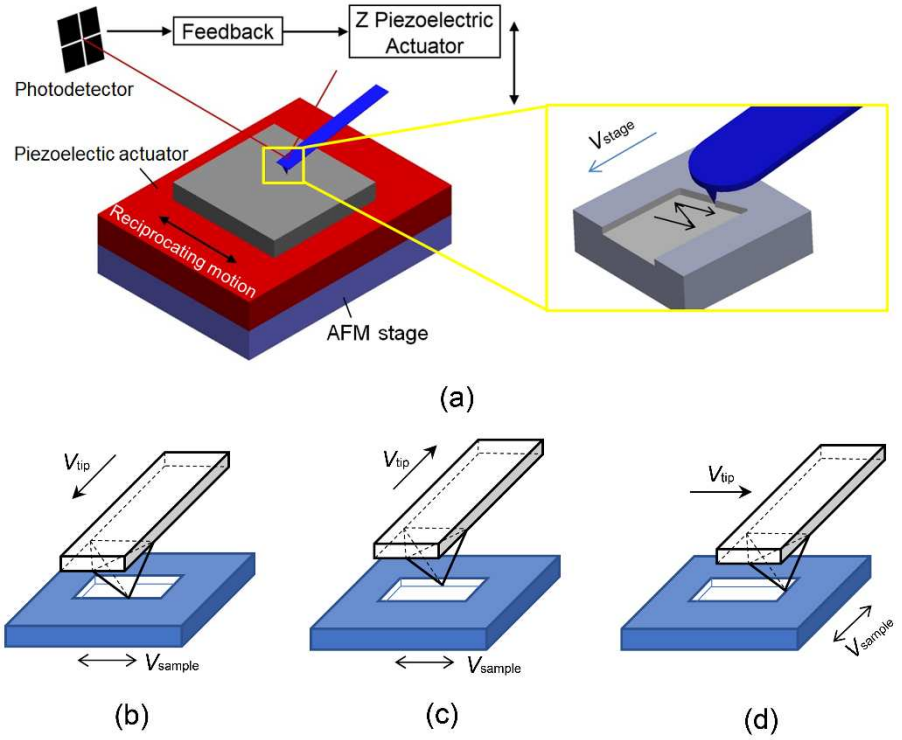

Fig. 1 (a) Schematic of the nanomachining set-up and typical relative movements between the AFM tip and the sample (b) edge-forward, (c) face-forward and (d) side-forward.

The piezoelectric actuator utilised in this study was driven by a signal amplifier (2100HF, Trek, USA) and a signal generator (WaveStation 2012, Teledyne LeCroy, USA). The voltage output produced by the signal generator was multiplied 50 times by the amplifier. A sinusoidal waveform was employed to control the amplitude and the frequency of the reciprocating motion of the piezoelectric actuator. The workpiece considered was an injection moulded PMMA sample with dimensions 10 mm x 10 mm x 3 mm. The arithmetical mean roughness, R_a, of the sample surface was less than 1 nm. This was measured from an AFM scan over a 20 μm by 20 μm area. It could be

reasonably assumed that, when machining PMMA, the wear of the diamond tip is negligible.

Based on this set-up, the procedure adopted to carry out the nanomachining of a groove on the surface of the PMMA workpiece was as follows:

(i) The AFM tip was first approached towards the sample to be machined until contact was made and a pre-set normal load of 20 μN was attained. This normal load corresponds to a given voltage output from the position sensitive photodetector (PSPD) of the AFM instrument. This value was then maintained throughout via the feedback loop of the AFM system by adjusting the vertical motion of the fixed end of the probe.

(ii) Next, in order to machine a groove, the stage of the AFM instrument was controlled to describe a linear trajectory, which was 36 μm in length and perpendicular to the reciprocating motions of the actuator. The speed of the stage during this step defined the feed value of a machining operation.

(iii) After cutting a groove, the normal load was reduced to 20 nN and the AFM stage was actuated to reach the starting position of the next groove to be cut. Once the tip was in the correct position to machine this subsequent groove, the normal load was increased again to 20 μN.

The applied normal load, F_N, the machining speed, v, and feed, Δ, could be determined based on the following expressions:

$$F_{\mathrm{N}} = K_{\mathrm{N}}.S.V_{\mathrm{A-B}} \quad (1)$$

$$\Delta = \frac{v_{\mathrm{stage}}}{2.f} \quad (2)$$

$$v = 2.f\sqrt{b^2 + \Delta^2} \quad (3)$$

where K_{N} is the cantilever normal spring constant, S is the vertical sensitivity of the PSPD and $V_{\mathrm{A-B}}$ is the pre-set target voltage value for the vertical signal on the PSPD. The velocity of the AFM stage is v_{stage}. Finally, the variables f and b are the frequency and the amplitude of the workpiece movement, respectively.

Following the completion of the machining trials, the 3D topography of the fabricated grooves was recorded using non-contact mode AFM scanning. For this, a new silicon probe (NSG30, NT-MDT, Russia) with a tip radius less than 10 nm was utilised. In addition, in order to provide additional data to analyse the machining results, the voltage output "A-B" and "C-D" on the PSPD and the signal sent by the controller to the AFM stage were also recorded. More specifically, the "A-B" and "C-D" signals provide information about bending and torsional motions, respectively, at the free end of the cantilever. A NI 9223 device from National instrument was employed to collect these signals through a signal access module (SAM) from Park Systems. A specially developed software was used to connect to the SAM and to

record the signals during the nanomachining experiments.

2.2. Characterisation of the piezoelectric actuator motions

The unidirectional piezoelectric actuator utilised is a critical component of the AFM set-up developed. Thus, the dynamic characterisation of its motion under a range of drive frequencies and voltages was studied first. This was carried out using a one-dimensional laser doppler vibrometer (LDV) (OFV-303, Polytec, Germany) when the PMMA sample was mounted on the actuator, as shown in Figure 2 (a). The LDV system operated with a laser wavelength of 633 nm and its resolution, stated by the manufacturer, was 32 nm when measuring the amplitude of the piezoelectric actuator motion under the experimental conditions used in this study. The laser beam of the LDV was directed onto the upper edge of the actuator in a direction parallel to its shearing motion. The amplitude of the reciprocating displacements was recorded online as voltage values by the controller of the LDV. Then, this voltage signal was converted into actual displacements based on the knowledge of the sensitivity of the controller. In this way, it was possible to determine the amplitude of the motion of the actuator as a function of the driving frequency and voltage, prior to the start of the nanomachining experiments.

Figure 2 (b) shows the measured amplitude of the piezoelectric actuator as a function of the driving frequency for an input peak-to-peak voltage of 225 V. Based on these data, the theoretical machining speed could be calculated for each frequency

value based on Eq. (3). In this study, the displacements of the actuator were measured in a configuration, where the mass of the PMMA workpiece was considered but the cutting loads were not taken into account. However, during tip-based nanomachining of polymers, such loads are typically less than 100 μN [18, 19] and thus can be assumed to be relatively small. For this reason, it can be assumed that the cutting loads could have only a minor effect on the dynamic characteristics of the piezoelectric actuator during actual nanomachining operations.

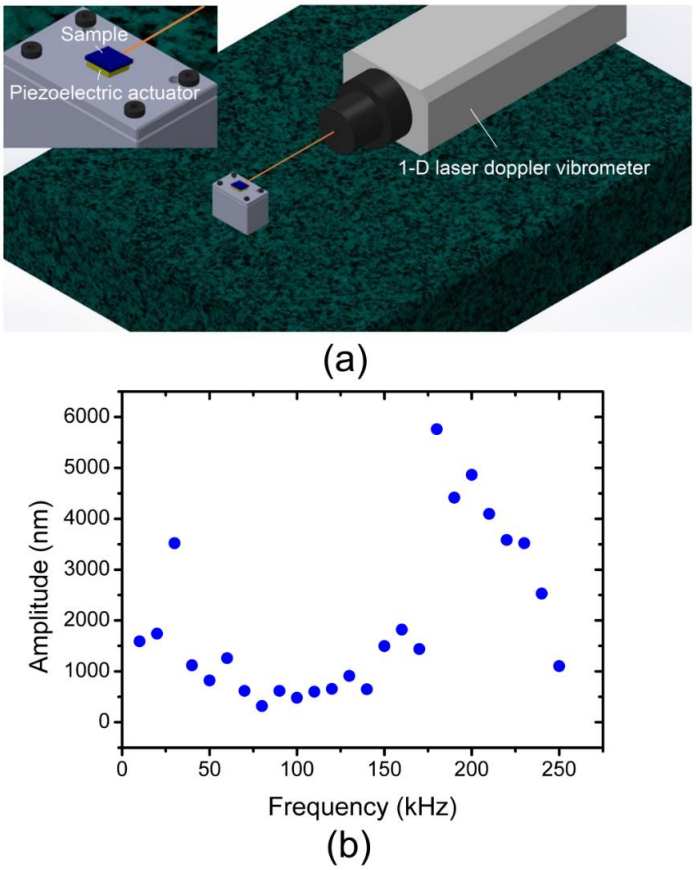

Fig. 2 (a) Illustration of the LDV set-up employed to characterise the dynamic displacements of the piezoelectric actuator and (b) measured amplitude of the piezoelectric actuator reciprocating motion as a function of the driving frequency for an input peak-to-peak voltage of 225 V.

3. Results and discussion

3.1 *Influence of the frequency on the machined grooves*

Our previous investigations suggest that both the cutting speed and the feed direction are critical parameters as they have important effects on the machining response of a polymer material [20, 21]. As described in Eq. (3), the cutting speed is mainly dependent on the frequency of the reciprocating motion and the width of the groove. Thus, in the present study, two typical frequencies of 10 kHz and 40 kHz were selected based on the data reported in Figure 2 (b). These correspond to amplitude values of 1590 nm and 1120 nm, respectively. The frequency of 10 kHz was considered as it was twice larger than the maximum frequency used by Gozen and Ozdoganlar [16], which was identified earlier as state-of-the art. Based on the data measured with the LDV, this should correspond to a theoretical cutting speed of 1.9 m/min. In addition, in order to push the theoretical cutting speed achieved over 5 m/min at the tip-workpiece interface, a frequency of 40 kHz was also selected which corresponds to a theoretical speed of 5.6 m/min. It was decided that this would be the highest frequency considered since the maximum velocity considered for the motion of the AFM stage was 400 μm/s and higher frequencies would have led to feed values, which would be too small, i.e. less than 1 nm. Finally, a low frequency of 10 Hz was also chosen to provide comparative data when the feed is much larger than the amplitude of the reciprocating motions. In this case, the cutting speed was much lower at only 6 mm/min.

When studying the influence of the frequency on the machining characteristics, the speed of the AFM stage was maintained constant at 100 μm/s. The average values for the machined depth and width as well as for the heights of the pile-up on both sides of the grooves are shown in Figure 3 for the range of frequencies considered. AFM scans of nano-scale grooves are shown in Figure 4, together with their cross-sections, for the case where the feed direction was 'edge-forward'. In addition, Figure 5 shows the corresponding SEM images of these grooves.

From Figure 3, it is observed that the smallest machined depths were obtained with the frequency of 10 Hz. Machining with a frequency of 10 kHz and 40 kHz could generate grooves which were around 4 times and 1.5 times deeper than those for 10 Hz, respectively. One reason for this observation may be that scratching at a very low frequency of 10 Hz results in a small velocity of the reciprocating motions of the tip (around 10 μm/s), which is negligible in comparison with the velocity of the AFM stage, which was 100 μm/s. In this case, there is no overlap between adjacent lateral tip trajectories along the width of the groove. As reported in [21], such an overlap contributes to the formation of deeper structures as the surface at the bottom of a groove can be processed more than once by the tip. Based on Eq. (2), the feed values for 10 kHz and 40 kHz were estimated to be smaller than or equal to 5 nm, which is about twenty times less than the radius of the AFM diamond tip. This results in the overlapping of the adjacent reciprocating trajectories for these higher frequencies. Thus, for a low frequency of 10 Hz, it could be said that the tip is machining in a configuration similar to that of conventional scratching, which relies

on the displacement of the stage only, albeit with the small difference that the reciprocating motions of the actuator still led to the formation of a slightly curved groove, see Figure 4 (a).

It is also observed from Figure 3, and from the cross sections in Figure 4 (d), that grooves machined with a frequency of 10 kHz were deeper than those processed at 40 kHz. Complementary SEM observations also revealed that only the grooves produced with 10 kHz were cut via shearing of the material with chip formation, see Figure 5 (b). Thus, the reduction of the contact area between the tip and the sample, as a result of the formation of chips, would consequently lead to an increase of the machined depth of the grooves processed at 10 kHz. In addition, based on the work reported in [22], it is anticipated that the transition from viscoelastic to viscoplastic behaviour has already taken place for the PMMA material for both frequency values of 10 kHz and 40 kHz. Indeed, in both cases, the cutting speed was higher than the threshold of 0.1 m/min taken from [22]. Thus, it is also expected from data given in [22] that a higher elastic recovery takes place when processing at 40 kHz, further reducing the groove depth. Regarding the formation of chips, which occurred only when processing at 10 kHz, it is suggested that this is a consequence of the influence of the feed. The feed values at a frequency of 10 kHz were four times higher than those for 40 kHz (i.e. 5 nm and 1.3 nm, respectively). Thus, the higher undeformed chip thickness should be beneficial for the generation of chips in the case of 10 kHz. Moreover, when the tip is following a zigzag scratching trajectory and the feed is much smaller than the width of the machined groove, a relatively large attack angle may also be a possible reason

for the chip formation as discussed in [21].

As shown in Figure 3, the heights of pile-ups on both sides of the grooves were almost identical at 10 Hz and 40 kHz when scratching with the ‘edge-forward’ feed direction. The possible reason for this can be due to the geometrical symmetry of the tip along the long axis of the probe cantilever. However, the height of the pile-up on the left side of the groove was much larger than that on the right side in the case of 10 kHz. Thus, the same explanation does not apply here. On the right side of the groove, the formation of chips should be the main reason for the decrease of the height of the pile-up. Thus, a slightly skewed orientation of the pyramidal base of the AFM tip and the inclination of the sample surface may be the possible reasons for the asymmetric pile-up on both sides of the groove.

Furthermore, it can be seen in Figure 3 that the width of the groove at 10 kHz is much larger than the groove width at 10 Hz or 40 kHz when scratching in the ‘edge-forward’ feed direction. A possible reason for this observation is that the amplitude of the reciprocating displacement generated by the piezoelectric actuator at 10 kHz was higher than that of 40 kHz, as shown in Figure 2 (b). In addition, at a frequency of 10 Hz, given that the processing condition is similar to that of conventional scratching, the width of the groove is only dependent on the geometry of the AFM tip. The second possible reason is that the machined depth at a frequency of 10 kHz was much larger than that at 10 Hz and 40 kHz, as seen in Figure 3. In this case, the AFM tip would have penetrated deeper into the material, which in turn

should lead to a larger groove width. The third factor that may influence the width of the grooves is the elastic recovery of the material. Based on the discussion reported earlier, it is expected that the elastic recovery is increased at the higher scratching frequency of 40 kHz.

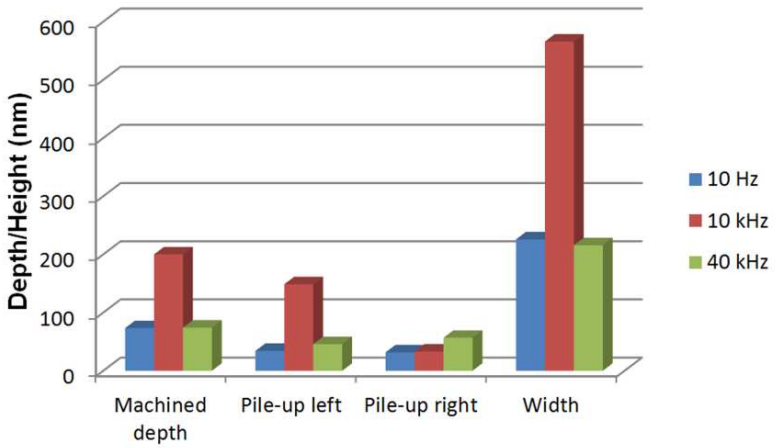

Fig. 3 Groove depth, height of the pile-up on the left side, height of pile-up on the right side and groove width as a function of the selected frequency, i.e. 10 Hz, 10 kHz and 40 kHz.

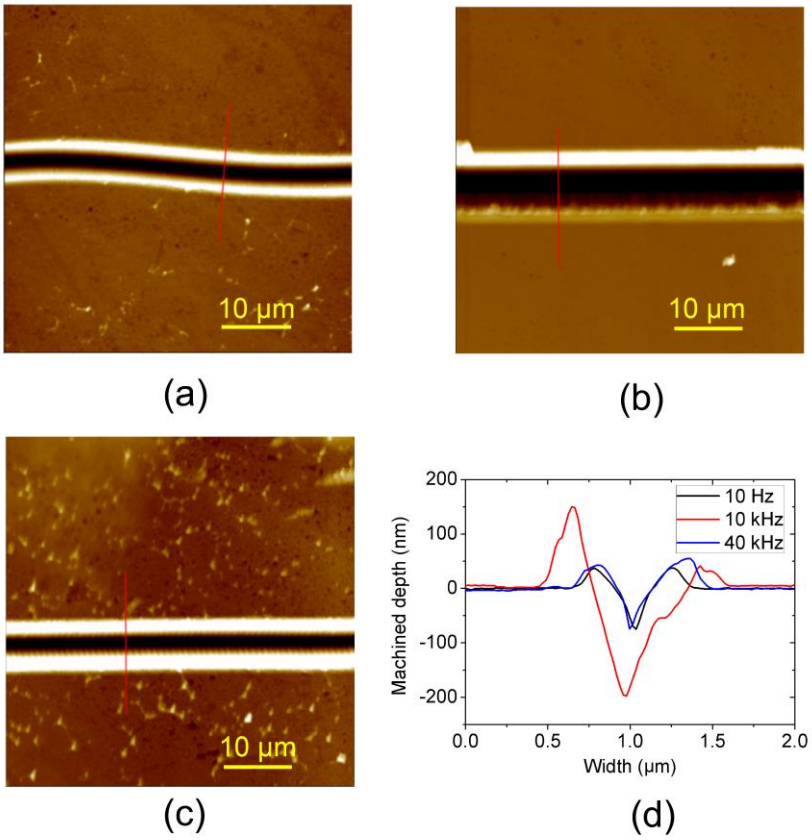

Fig. 4 AFM images of machined grooves with different frequencies: (a) 10 Hz, (b) 10 kHz, (c) 40 kHz for a stage velocity of 100 μm/s along the 'edge-forward' feed direction and (d) corresponding groove cross-sections.

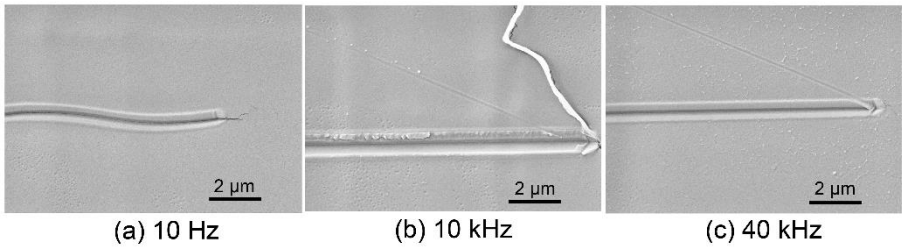

Fig. 5 SEM images of machined grooves with different frequencies: (a) 10 Hz, (b) 10 kHz and (c) 40 kHz for a stage velocity of 100 μm/s along the 'edge-forward' feed direction.

3.2 *Influence of the feed direction on the machined grooves*

Three feed directions were studied, namely 'edge-forward', 'face-forward' and 'side-forward', as described in Section 2.1. The speed of the AFM stage was maintained constant at 100 μm/s in this case. The average values for the machined depth and width as well as the heights of the pile-up on both sides of the grooves are given in Figure 6 for different feed directions and frequencies. It can be observed from Figure 6 (a) that the machined depths of the grooves obtained along the 'face-forward' feed direction are much smaller than those with the 'edge-forward' and 'side-forward' configurations. At a frequency of 10 Hz, given that the configuration of the cutting process is similar to that of conventional tip-based nanomachining, the feed direction essentially corresponds to the scratching direction. In previous studies [23, 24], it was reported that this parameter has a large influence on the machining outcomes, such as the machined depth, cutting state and the chip formation. In particular, for a given set normal load, as a result of the deflection of the cantilever during processing and the working principle of the AFM feedback loop, scratching with the 'edge-forward' direction results in a larger actual normal load applied on the sample surface. On the other hand, a smaller actual normal load occurs along the 'face-forward' configuration [23]. Moreover, the contact area between the tip and the sample is relatively large when scratching in the 'face-forward' case, as discussed in [23]. Based on these factors, the machined depth for the 'face-forward' feed direction is expected to be the smallest among the three cases considered when processing with the frequency of 10 Hz. This was indeed observed experimentally (c.f. Figure 3 (a)).

For the frequencies of 10 kHz and 40 kHz, the machined depths obtained with the ‘edge-forward’ and ‘side-forward’ feed directions are around 3 or 4 times larger than that achieved with the ‘face-forward’ feed direction. Figure 7 shows the AFM images and the corresponding cross-sections of the grooves obtained with different feed configurations at 10 kHz. The corresponding SEM micrographs are given with Figure 8. In particular, it can be seen from this figure that chips could be generated with both the ‘edge-forward’ and ‘side-forward’ feed directions, while no chip was formed for the ‘face-forward’ operation. In this case, the change of deflection of the cantilever and of the contact area between the tip and sample material caused by the different feed directions can also be considered as a factor for the various machined depths reported in Figure 6. Moreover, due to the zigzag tip trajectory, different feed directions can lead to different cutting angles during the scratching process [19]. As discussed in the previous section, the relatively high cutting speed and large attack angle when scratching in the ‘edge-forward’ configuration can lead to chip formation. For the ‘face-forward’ case, the attack angle of the main cutting edge of the diamond AFM tip is very small [21], which can result in ploughing being the dominant machining phenomenon and lead to the decrease of the machined depth.

As shown in Figure 6 (b) and (c), it can be found that the heights of the material pile-up for both sides of the grooves processed in the ‘face-forward’ feed direction are relatively small compared to the other directions. This is attributed to the comparatively limited volume of material removal. Furthermore, in the ‘face-forward’ case, the widths of the grooves scratched at 10 kHz and 40 kHz are similar, which is

around twice larger than that obtained by 10 Hz. The possible reason for this phenomenon can be explained as follows. First, the width of the groove scratched at a frequency of 10 Hz is mainly dependent on the geometry of the AFM tip and the recovery rate of the polymer material. At the frequencies of 10 kHz and 40 kHz, the amplitude of the reciprocating displacement generated by the piezoelectric actuator plays an important role in the machining process, as so the widths obtained at 10 kHz and 40 kHz are therefore larger. Moreover, the materials extrusion state by the AFM tip in the case of the 'face-forward' feed direction is different from that of the 'edge-forward' and 'side-forward' feed directions, which may lead to different material recovery rate for different scratching speeds. Thus, this may be one of the factors for the similar widths of the grooves scratched using the frequencies of 10 kHz and 40 kHz with the 'face-forward' feed direction.

Figure 6 (a) also reveals that, for the 'side-forward' configuration, the machined depth at 10 kHz is slightly smaller than that obtained in the 'edge-forward' case. The possible reason behind this observation can be due to the asymmetrical geometry of the AFM diamond tip. Indeed, this should result in the trace and retrace paths of the reciprocating motion between the tip and the sample exhibiting different cutting states. In particular, for the trace path of this motion, the tip is mainly scratching along the 'edge-forward' direction. In this case, the deflection of the cantilever of the AFM tip can result in the increase of the actual normal load applied on the sample surface, which can lead to the formation of the chips. This hypothesis seems to be supported by the SEM micrograph shown in Figure 8 (c). In the case of the retrace path of the

reciprocating motion however, the tip is mainly scratching along the 'face-forward' direction. As a result, the actual normal load applied on the sample surface can be reduced [23], which, in turn, can result in less material being pushed on the right side of the groove as shown in Figure 7 (c). Therefore, due to the periodic occurrence of the ploughing and cutting machining states for the 'side-forward' configuration, ridges can be generated on one side of the groove, as shown in Figure 8 (c). Moreover, the intermittent extrusion of the material and the deflection of the cantilever may lead to the adhesion of the formed chips to one side of the groove. Thus, the height of the material pile up on the left side is much larger than that on the right side of the groove, as shown in Figure 7 (c) and observed when comparing the plots of Figure 6 (b) and Figure 6 (c).

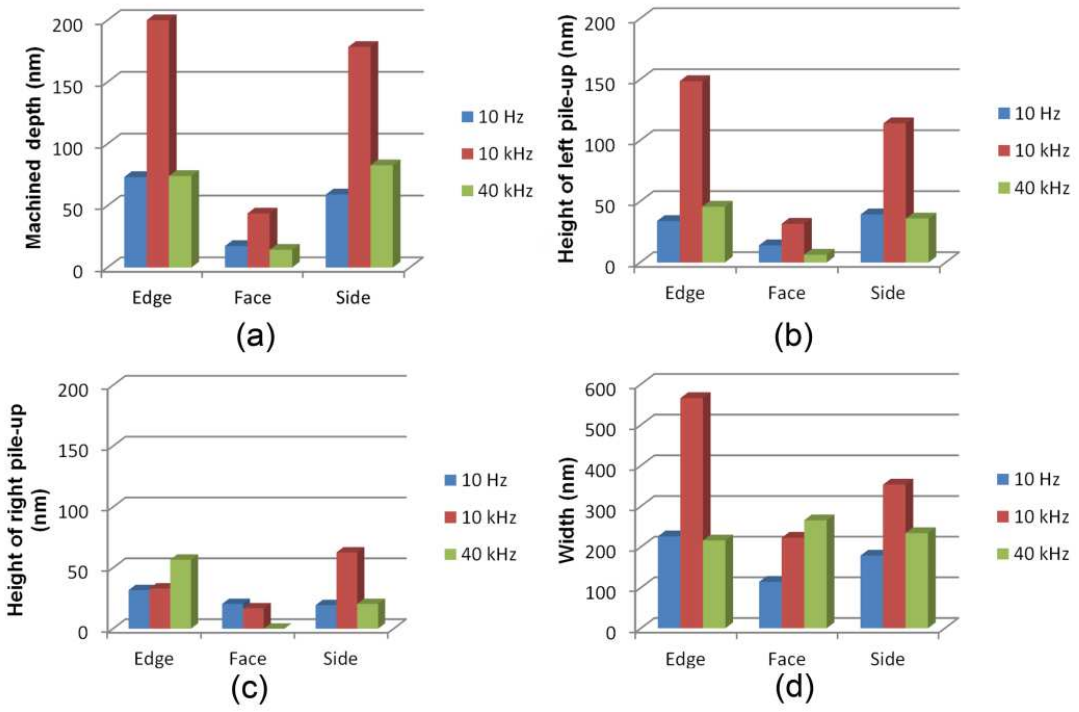

Fig. 6 (a) Groove depth, (b) height of the pile-up on the left side, (c) height of pile-up on the right side and (d) groove width as a function of the selected frequency (10 Hz,

10 kHz and 40 kHz) and feed direction (edge-, face- and side-forward).

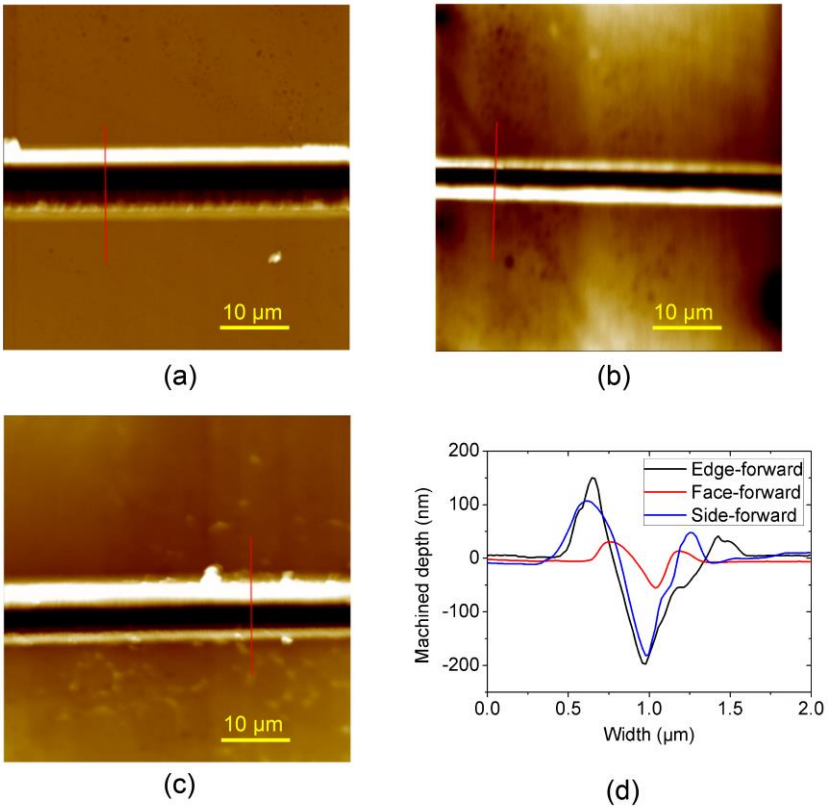

Fig. 7 AFM images of machined grooves with different feed directions: (a) 'edge-forward', (b) 'face-forward', (c) 'side-forward' for a stage velocity of 100 µm/s and a frequency of 10 kHz and (d) corresponding groove cross-sections.

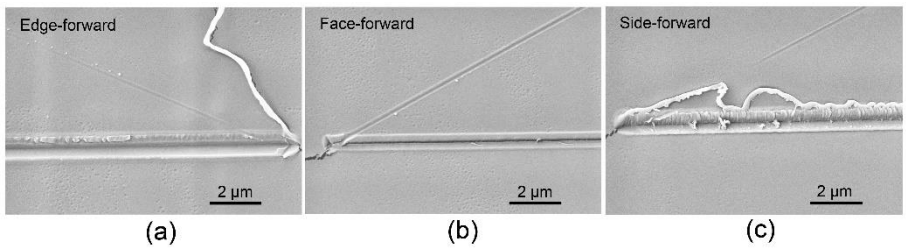

Fig. 8 SEM images of machined grooves with different feed directions: (a) 'edge-forward', (b) 'face-forward', (c) 'side-forward' for a stage velocity of 100 µm/s and a frequency of 10 kHz.

3.3 *Influence of cutting loads on the machined grooves*

Figure 9 shows the original (OS) and after filtering (AF) evolution of the voltage signals along the vertical (A-B) and horizontal (C-D) axes of the PSPD. The displacement signal (DS) along the moving axis of the AFM stage is also given as a reference to show when the AFM tip is actually moving along the groove length. The A-B signal of the PSPD represents the deflection of the cantilever probe in the vertical direction, which reflects the change of the actual normal load applied on the sample. The C-D signal of the PSPD shows the torsion of the cantilever, which reflects the change of the lateral force applied on the apex of the AFM probe. In this study, the AFM tip first approaches the sample surface before the piezoelectric actuator is driven to achieve reciprocating motions. Thus, the first inflection points of both the A-B and C-D signals shown in Figure 9 correspond to the AFM tip penetrating into the sample material until the pre-set normal load of 20 μN is reached. After this point, the amplitude of the A-B signal (see the OS for the A-B trace in Figure 9 (c)) increases quite significantly for the 'side-forward' feed direction. This should be the result of the reciprocating motion of the sample, which is along the long axis of the cantilever in this case. Indeed, after the increase in normal load, it is expected that there will be two different bending moments for one cycle of reciprocation motion. Thus, this will lead to different cantilever deflections for each trace and retrace path in one cycle. The opposite phenomenon is observed for the C-D signal (see the OS for the C-D trace in Figure 9 (c)). This is due to the fact that the reciprocating motion of the actuator, before machining starts along the groove length, has no effect on the torsion

of the cantilever in this configuration.

The first inflection point along the DS signal, which records the linear motion of the AFM stage, shows the starting point of the scratching process along a groove. The second inflection point for this signal represents the end of this linear motion, which means that the tip has reached the end of the groove. Based on the knowledge of the start of the scratching process, the A-B and C-D signals then can be analysed for different feed directions. In this way, it is first observed that the A-B signal displays almost no variation for the feed directions 'edge-forward' and 'face-forward' except at the very beginning of the groove. This specific event occurs because the bending moment at the free end of the cantilever changes relatively rapidly during the short time interval upon the initiation of the stage motion. Following this, the amplitude of the OS trace of the A-B signal remains similar to that before the stage motion indicating that the amplitude of the bending moment keeps constant throughout the machining of the groove. However, for the 'side-forward' feed direction, it can be seen from Figure 9 (c) that the amplitude of both the A-B and C-D signals increases along the length of the groove. This coincides with the fact that a chip was formed only at the beginning of the groove, as seen in Figure 8 (c). Thus, once the process changes from being cutting-dominated to ploughing-dominated, the magnitude of the load acting on the tip became larger. In general, the value of the A-B signal after filtering (see the AF traces in Figure 9) for the three feed directions is the similar before and after the start of machining because the feedback loop of the AFM system was always switched on.

It can also be seen from Figure 9 that the amplitude of the C-D signal for the ‘edge-forward’ feed direction increases upon initiation of machining along the groove, while it decreases for the ‘face-forward’ feed direction. The higher machined depth during the scratching process along the ‘edge-forward’ feed direction may lead to a larger torsion of the cantilever in comparison with that along the ‘face-forward’ feed direction. The value of the C-D signal after filtering shows no change before and after the scratching process for both the ‘edge-forward’ and ‘face-forward’ feed directions due to symmetric geometry of the diamond tip along these two configurations. On the other hand, for the ‘side-forward’ case, only one main cutting edge takes part in the process. This can result in a difference in the lateral force applied on the apex of the tip between the trace and the retrace paths, particularly if different machining states take place for each path. In addition, due to the feed direction being perpendicular to the long axis of the cantilever, a change of the value of the C-D signal after filtering can be seen with Figure 9 (c). Therefore, the behaviour of the different signals shown in Figure 9 agrees well with the machining states and results discussed in the previous sections.

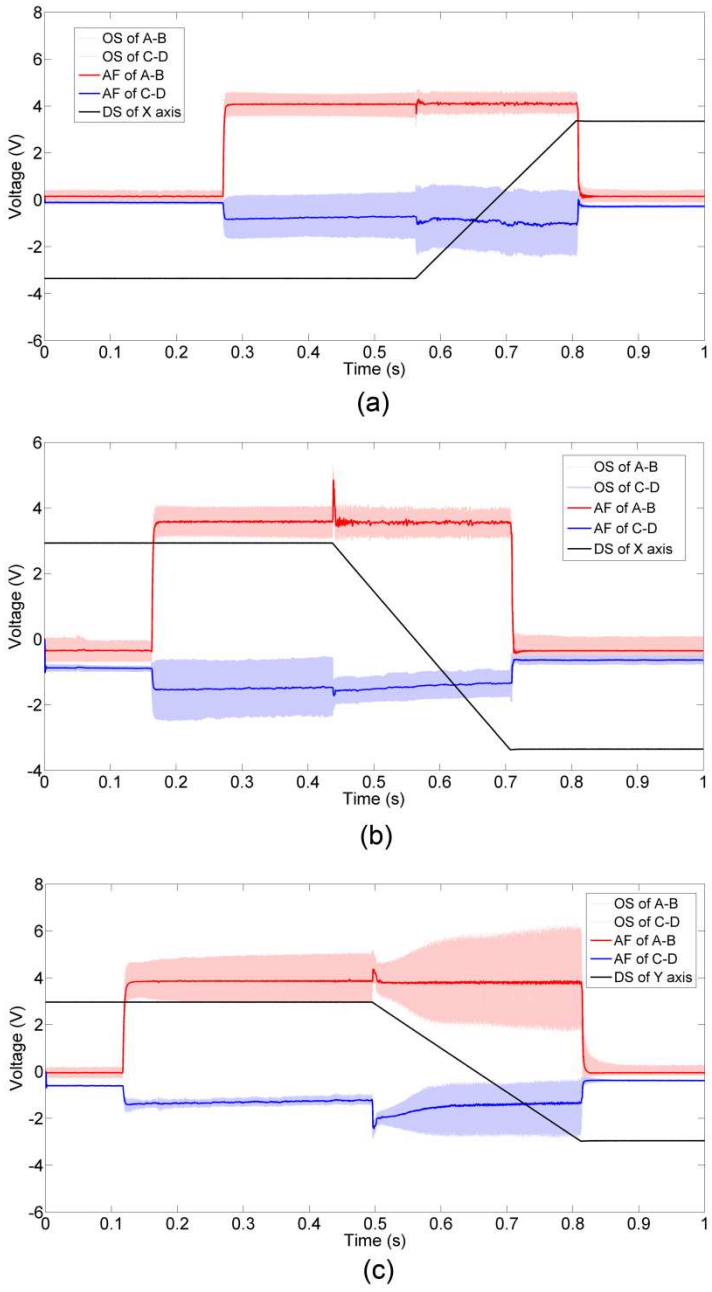

Fig. 9 Original (OS) and after filtering (AF) evolution of the voltage signals along the vertical (A-B) and horizontal (C-D) axes of the PSPD and stage displacement signal (DS) for different feed directions: (a) ‘edge-forward’, (b) ‘face-forward’, (c) ‘side-forward’ for a stage velocity of 100 μm/s and a frequency of 10 kHz.

3.4 *Influence of the feed on the machined grooves*

As shown in Eq. (2), the value for the feed utilised can be determined based on the frequency of the actuator reciprocating motions and on the velocity of the AFM stage. Thus, for a given frequency, the speed of the AFM stage was varied to study the influence of the feed on the machined groove. In particular, the stage velocity values of 100 μm/s, 200 μm/s and 400 μm/s were considered. In this case, the frequency and the feed direction selected were 10 kHz and 'edge-forward', respectively. The feed values for each stage velocity were calculated to be 5 nm, 10 nm and 20 nm, respectively. Besides, the theoretical cutting speed at the tip-material interface could be considered constant at 1.9 m/min due to the minor influence of the stage velocity in this processing window.

The depths, heights of the material pile-up and the widths of the machined grooves are shown in Figure 10 as a function of the feed value utilised. In addition, Figure 11 and Figure 12 report the corresponding AFM and SEM images of the obtained grooves. It can be observed from Figure 10 that the machined depth decreases with the increase of the feed. Consequently, the width and the pile-up formed should follow the same trend. This can be verified in Figure 10 although this result does not apply for the pile-up on the right side of the groove. The much smaller pile-up on this side for feed values of 5 nm and 10 nm should be due to the fact that continuous chips were formed along one side of the grooves as reported with Figure 12 (a) and (b). Finally, it can be seen from Figure 12 (c) that no chips were observed

with the highest feed value of 20 nm but some periodic structures are found instead on both sides of the groove. The period of these structures is around 200 nm, which is 10 times the feed value. This indicates that the tip scratched for 10 cycles of reciprocating motion to generate one such structure. Because the period of these structures is relatively large, it is hypothesised that the materials displaced for one period cannot adhere with that of another period in order to form a continuous chip. As a result, a large height of the material pile-up can be found on the right side of the groove with the feed value of 20 nm, see Figure 10.

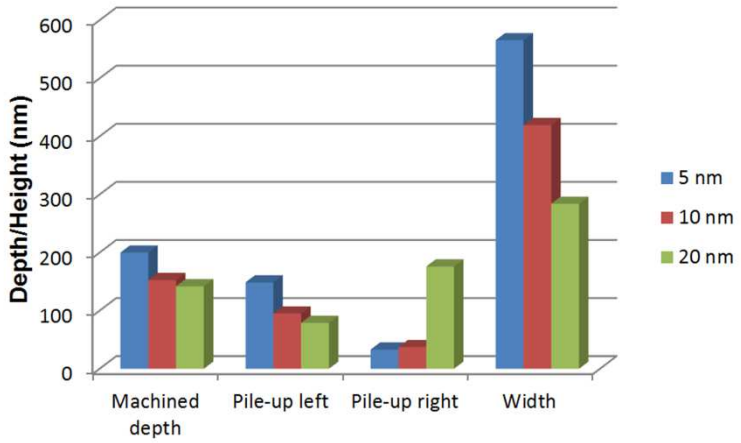

Fig. 10 Groove depth, height of pile-up on the left side, height of pile-up on the right side and width as a function of the feed (5 nm, 10 nm and 20 nm).

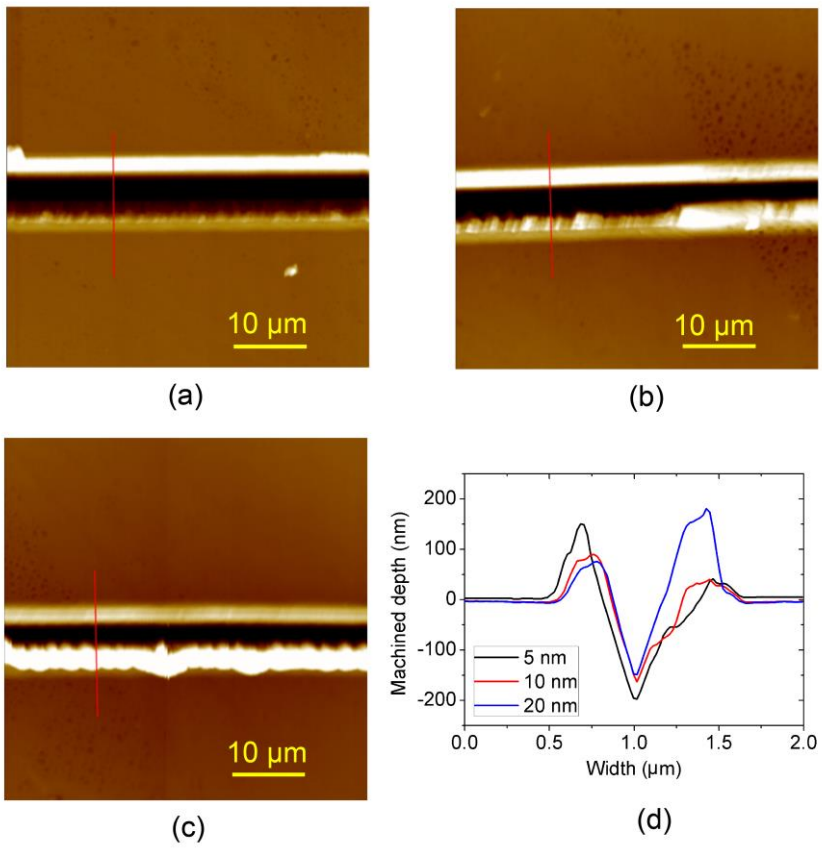

Fig. 11 AFM images of machined grooves with different feed values: (a) 5 nm, (b) 10 nm, (c) 20 nm for the 'edge-forward' configuration and a frequency of 10 kHz, (d) corresponding groove cross-sections.

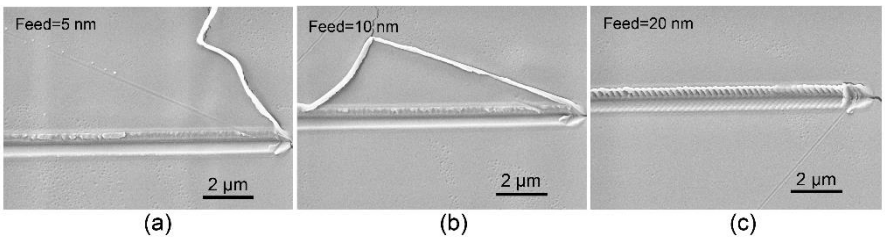

Fig. 12 SEM images of machined grooves with different stage velocities: (a) 5 nm, (b) 10 nm, (c) 20 nm for the 'edge-forward' configuration and a frequency of 10 kHz.

4. Conclusions

In this study, a modified AFM set-up was developed to increase the speed of the AFM tip-based nanomachining process at the interface between the tool and the workpiece. This was achieved by combining fast reciprocating motions of a shear-type piezoelectric actuator, on which the workpiece was mounted, and linear displacements of the AFM stage. The motions of the actuator utilised were characterised using a 1-D laser doppler vibrometer prior to the nanomachining experiments. Based on the dynamic characterisation of the actuator, it was estimated that a theoretical cutting speed just over 5 m/min may be achieved for a frequency of 40 kHz, which represents a significant increase compared to current AFM tip-based nanomachining. Potential future directions for work could be to investigate the influence of the cutting loads on the amplitude of the generated actuator displacements.

Grooves were successfully machined for all processing conditions investigated. The effect of different feed and cutting speed values as well as of three feed directions on the machined depth and on the generation of chips was also studied in detail. This initial investigation, which was conducted on PMMA, suggests that the chip formation process is sensitive to the feed and the feed direction employed, which in turn should influence the depth of the machined grooves. In particular, chips were more likely to be formed in the PMMA material along the edge forward configuration and when the feed was between 5 nm and 10 nm. This work provides a route for

adaptation of commercial AFM systems to achieve high cutting speeds for nano-electro-mechanical systems and related semiconductor devices.

Acknowledgements

The reported research was funded by the Engineering and Physical Sciences Research Council (EPSRC) under the grant EP/M020703/1. All data created during this research are openly available from Cardiff University data archive at http://doi.org/10.17035/d.2017.0040949516.

References

[1] A.A. Tseng, "Removing material using atomic force microscopy with single- and multiple-tip sources," Small, 2011; 7(24): 3409-3427.

[2] Y.D. Yan et al., "Recent advances in AFM tip-based nanomechanical machining," Int. J. Mach. Tools & Manuf., 2015; 99: 1-18.

[3] X.N. Xie et al., "Nanoscale materials patterning and engineering by atomic force microscopy nanolithography," Mat. Sci. Eng., 2006; R54: 1-48.

[4] Y. Yan et al., "A control approach to high-speed probe-based nanofabrication," Nanotechnology, 2009; 20(17): 175301 (11 pages)

[5] K. Bourne et al., "Study of a high performance AFM probe-based microscribing process," ASME Trans., J. Manuf. Sci. and Eng., 2010; 132(3): 030906 (10 pages).

[6] Y. He et al., "Fabrication of periodic nanostructures using dynamic plowing

lithography with the tip of an atomic force microscope," Appl. Surf. Sci., 2018; 427: 1076-1083.

[7] L. Chen et al., "Sliding speed-dependent tribochemical wear of oxide-free silicon," Nanoscale Research Letters, 2017; 12: 404 (7 pages).

[8] F. Tian et al., "Fast tool servo diamond turning of optical freeform surfaces for rear view mirrors," Int. J. Adv. Manuf. Technol., 2015; 80 (9): 1759-1765.

[9] M. Tauhiduzzaman et al., "Effect of material microstructure and tool geometry on surface generation in single point turning," Precision Engineering, 2014; 38 (3): 481-491.

[10] M. Chen et al., "Study on the optical performance and characterization method of texture on KH_2PO_4 surface processed by single point diamond turning," Applied Surface Science, 2013; 279: 233-244.

[11] A. M. Elkaseer et al., "Modelling the surface generation process during AFM probe-based machining: simulation and experimental validation," Surface Topography: Metrology & Properties, 2014; 2 (2): 025001.

[12] A. D. L. Humphris et al., "A mechanical microscope: High-speed atomic force microscopy," Applied Physics Letters, 2005; 86 (3): 034106.

[13] L. M. Picco et al., "Breaking the speed limit with atomic force microscopy" Nanotechnology, 2007; 18 (4): 044030.

[14] Y. D. Yan et al., "Investigation on AFM-based micro/nano-CNC machining system," Int. J. Mach. Tools & Manuf., 2007; 47: 1651-1659.

[15] E. B. Brousseau et al., "A hybrid roll-to-roll AFM set-up for high throughput

tip-based nano-machining," Manuf. Lett., 2015; 6: 10-13.

[16] B. A. Gozen et al., "Design and evaluation of a mechanical nanomanufacturing system for nanomilling," Prec. Eng., 2012; 36(1): 19-30.

[17] L. Zhang et al., "High-rate tunable ultrasonic force regulated nanomachining lithography with an atomic force microscope," Nanotechnology, 2012; 23: 085303 (9 pages).

[18] S. S. Park et al., "Vibration assisted nano mechanical machining using AFM probe," CIRP Annals – Manuf. Tech., 2014; 63: 537–540.

[19] Y. Geng et al., "Investigation of the nanoscale elastic recovery of a polymer using an atomic force microscopy-based method," Meas. Sci. Technol. 2016; 27: 015001.

[20] Y. Geng et al., "Investigation on friction behavior and processing depth prediction of polymer in nanoscale using AFM probe-based nanoscratching method," Tribology International, 2017; 114: 33-41.

[21] Y. Geng et al., "Processing outcomes of the AFM probe-based machining approach with different feed direction," Precision Engineering, 2016; 46: 288-300.

[22] N. Aleksy et al., "Numerical study of scratch velocity effect on recovery of viscoelastic-viscoplastic solids," Int. J. Mech. Sci. 2010; 52: 455-463.

[23] Y. Geng et al., "Effect of cantilever deformation and tip-sample contact area on AFM nanoscratching," J. Vac. Sci. Technol. B 2013; 31 (6): 061802.

[24] A. A. Tseng et al., "Scratch direction and threshold force in nanoscale scratching using atomic force microscopes," Applied Surface Science, 2011; 257: 9243-9250.